HHS Public Access

Author manuscript

Nat Methods. Author manuscript; available in PMC 2011 October 12.

Published in final edited form as:

Nat Methods. 2011 September ; 8(9): 745–752.

Cell-type Specific Optogenetic Mice for Dissecting Neural Circuitry Function

Shengli Zhao[1,9], **Jonathan T. Ting**[1,2,9], **Hisham E. Atallah**[2], **Li Qiu**[1], **Jie Tan**[3], **Bernd Gloss**[1,4], **George J. Augustine**[5,6,7], **Karl Deisseroth**[8], **Minmin Luo**[3], **Ann M. Graybiel**[2], and **Guoping Feng**[1,2]

[1]Department of Neurobiology, Duke University Medical Center, Durham NC 27710, USA

[2]McGovern Institute for Brain Research and Department of Brain and Cognitive Sciences, MIT, Cambridge, MA 02139, USA

[3]National Institute of Biological Sciences, Beijing, 102206, China

[4]Duke NeuroTransgenic Laboratory, Duke University Medical Center, Durham NC 27710, USA

[5]Center for Functional Connectomics, Korea Institute of Science and Technology, 39-1 Hawolgokdong, Seongbukgu, Seoul, 136-791 Republic of Korea

[6]Program in Neuroscience and Behavioral Disorders, Duke-NUS Graduate Medical School, 8 College Road, Singapore 169857, Singapore

[7]A*STAR/Duke-NUS Neuroscience Research Partnership, 61 Biopolis Drive, Proteos, Singapore 138673, Singapore

[8]Department of Bioengineering, Stanford University, CA 94305, USA

Abstract

Optogenetic methods have emerged as powerful tools for dissecting neural circuit connectivity, function, and dysfunction. We used a Bacterial Artificial Chromosome (BAC) transgenic strategy

Corresponding author – Guoping Feng (fengg@mit.edu).

[9]These authors contributed equally to this work.

RESOURCE SHARING NOTES: The cell-type specific ChR2-EYFP BAC transgenic mouse lines developed in this study have been deposited to the Jackson Laboratory and are under development for future distribution. The stock numbers, official stock names, and links to the Jackson Laboratory strain info web pages are provided below: *VGAT-ChR2-EYFP* Stock# 014548 B6.Cg-Tg(Slc32a1-COP4*H134R/EYFP)8Gfng/J http://jaxmice.jax.org/strain/014548.html *ChAT-ChR2-EYFP* line 6 Stock# 014546 B6.Cg-Tg(Chat-COP4*H134R/EYFP)6Gfng/J http://jaxmice.jax.org/strain/014546.html *ChAT-ChR2-EYFP* line 5 Stock# 014545 B6.Cg-Tg(Chat-COP4*H134R/EYFP)5Gfng/J http://jaxmice.jax.org/strain/014545.html *TPH2-ChR2-EYFP* Stock# 014555 B6;SJL-Tg(Tph2-COP4*H134R/EYFP)5Gfng/J http://jaxmice.jax.org/strain/014555.html *Pvalb-ChR2-EYFP* Stock# 012355 B6;SJL-Tg(Pvalb-COP4*H134R/EYFP)15Gfng/J http://jaxmice.jax.org/strain/012355.html

AUTHOR CONTRIBUTIONS G.F., K.D., and G.J.A. initiated the project as a joint collaboration to create novel ChR2 BAC transgenic mice as a resource for the neuroscience community. K.D. initially provided ChR2(H134R) DNA constructs. S.Z., L.Q., and B.G. generated the ChR2 BAC transgenic founder lines. S.Z. and L.Q. screened the founder lines. S.Z. performed all confocal imaging experiments. J.T.T. performed electrophysiological recordings and performed data analysis and interpretation for acute brain slice experiments for all mouse lines in the Feng Lab. J.T. performed electrophysiological recordings, and M.L. and J.T. performed data analysis and interpretation for acute brain slice experiments on *ChAT-ChR2-EYFP* line 6 and *VGAT-ChR2-EYFP* line 8 mice in the Luo Lab. H.E.A. performed *in vivo* electrophysiology, and H.E.A. and A.M.G. performed data analysis and interpretation for the *in vivo* electrophysiology data on *ChAT-ChR2-EYFP* line 6 mice in the Graybiel Lab. J.T.T. and G.F. wrote the manuscript.

to express Channelrhodopsin2 (ChR2) under the control of cell-type specific promoter elements. We provide a detailed functional characterization of the newly established *VGAT-ChR2-EYFP*, *ChAT-ChR2-EYFP*, *TPH2-ChR2-EYFP* and *Pvalb-ChR2-EYFP* BAC transgenic mouse lines and demonstrate the utility of these lines for precisely controlling action potential firing of GABAergic, cholinergic, serotonergic, and parvalbumin+ neuron subsets using blue light. This resource of cell type-specific ChR2 mouse lines will facilitate the precise mapping of neuronal connectivity and the dissection of the neural basis of behavior.

Keywords

Channelrhodopsin-2; ChR2-EYFP; ChR2(H134R); VGAT; ChAT; TPH2; Parvalbumin; Pvalb; electrophysiology; acute brain slice; dorsal raphe nucleus; Purkinje cells; thalamic reticular nucleus; striatal cholinergic neurons; cortical fast-spiking interneurons; hippocampal interneurons; bacterial artificial chromosome; BAC; transgenic mice

INTRODUCTION

Optogenetic strategies for controlling neuronal function are being widely implemented for dissecting neural connectivity, function, and dysfunction. Toward this end, it is crucial to target optogenetic constructs to defined neuronal subsets within complex brain circuits. A variety of approaches including *in utero* electroporation[1, 2] and *in vivo* injections of viral vectors[3–18] have been used to gain important insights into mammalian nervous system function using Channelrhodopsin-2 (ChR2). These delivery methods can prove labor-intensive and technically challenging, and thus the availability of transgenic animals with stable high-level expression of ChR2 in defined neuronal populations would greatly facilitate progress in this field.

We previously generated ChR2 transgenic mouse lines that express functional ChR2 in subsets of neurons throughout the nervous system[19, 20]. These lines have been employed in a variety of studies[13]. Subsequent studies have reported additional transgenic rodent lines, including *Thy1.2-ChR2* rats with expression in retinal ganglion cells[21], *Vglut-ChR2-EYFP* mice with expression in spinal cord and hindbrain[22], *OMP-ChR2-EYFP* mice with expression in olfactory sensory neurons[23], and α*CaMKII-tTA*∶∶*BTR6* mice with expression in striatal medium spiny neurons (MSNs)[24]. Collectively, these lines enable optogenetic control of some defined neuronal cell types, though clearly additional lines are required to further access the diverse classes of neurons and circuits throughout the nervous system.

Here, we employed a BAC transgenic strategy to express ChR2(H134R)-EYFP under the control of cell-type specific promoter elements to enable functional activation of GABAergic, cholinergic, serotonergic, and parvalbumin-(Pvalb) positive neuronal populations with blue light.

RESULTS

VGAT-ChR2(H134R)-EYFP transgenic mice

The vesicular γ-aminobutyric acid (GABA) transporter (VGAT) is specifically expressed in GABAergic neurons and glycinergic neurons[25, 26]. To express ChR2-EYFP in these inhibitory neurons, we targeted ChR2-EYFP to exon I of the VGAT gene (see Supplementary Fig. 1 for general targeting strategy). Four of ten founder lines exhibited a virtually indistinguishable ChR2-EYFP expression pattern throughout the brain, though with variable expression level. We pursued characterization of *VGAT-ChR2-EYFP* line 8 because it showed the strongest ChR2-EYFP expression (Supplementary Table 1). Whole brain sagittal images revealed strong ChR2-EYFP expression in the glomerular and mitral cell layer of the olfactory bulb, thalamic reticular nucleus (TRN), superior and inferior colliculus, the molecular layer of cerebellum and brainstem. Moderate ChR2-EYFP expression levels were also detected in the cortex, hippocampus, thalamus and the granule cell layer of the olfactory bulb (Supplementary Fig. 2a and Supplementary Fig. 3a–k). Co-immunostaining of GAD67 and EYFP showed clear colocalization throughout the brain (Supplementary Fig. 2b–d). Co-localization of GAD67+ neurons with ChR2-EYFP was 93% (cortex), 93% (hippocampus), 88.6% (inferior colliculus) and 100% (Purkinje cells). The vast majority of the ChR2-EYFP+ neurons were GAD67 positive (Supplementary Table 3), suggesting the ChR2-EYFP expressing neurons in this line are indeed inhibitory neurons.

To confirm that ChR2 in the *VGAT-ChR2-EYFP* line is functional, we performed electrophysiological recordings in acute brain slices from young adult mice. Cortical interneurons were targeted for recordings by visualization of membrane targeted EYFP fluorescence, readily detected at the somata (Fig. 1a). Delivery of blue light through an optic fiber positioned just above the recorded neurons elicited robust photocurrents (Fig. 1b). In the current-clamp mode, a 1s blue light stimulus caused high frequency repetitive action potential firing with no accommodation in the majority of recorded cortical interneurons, suggesting that these were putative fast-spiking interneurons. Further analysis revealed that these cortical interneurons were able to sustain high fidelity, high frequency firing in response to prolonged bouts of patterned blue light stimulation at 20 Hz (Fig. 1c). We next assessed the fidelity of action potential firing across a range of blue laser stimulation frequencies. At low frequencies the neurons responded with reliable action potential firing; however, extra spikes were commonly observed (Fig. 1d), which has previously been shown to be due to slow off kinetics of the WT and H134R variant of ChR2[27]. Extra spikes were reduced as stimulation frequency increased, and surprisingly, the majority of ChR2-expressing cortical interneurons were able to fire action potentials with perfect fidelity up to 80 Hz (Fig 1e).

To address the functionality of the ChR2 in the context of local cortical circuitry we recorded from cortical layer V pyramidal neurons that lack ChR2 expression. Pyramidal neurons were made to fire repetitively by constant current injection, and blue light was applied to the surrounding region to activate nearby ChR2-expressing interneurons (Fig. 1f). Cortical neuron firing was strongly suppressed by constant blue light or pulse trains of blue light at 50 Hz (Fig. 1g). Acute application of various synaptic blockers demonstrated that the

inhibition of pyramidal neuron firing required activation at both GABA-A and GABA-B receptors (Fig. 1h,i).

We extended our functional analysis of *VGAT-ChR2-EYFP* line 8 to hippocampal interneurons identified by bright EYFP fluorescence at the somata (Fig. 2a). All recorded hippocampal interneurons exhibited robust photocurrents (Fig. 2b,c), and the vast majority also fired action potentials in response to blue light. Interneurons in the CA1 and dentate gyrus regions responded with high fidelity to blue light up to 20 Hz (Fig. 2d,e,f), and some interneurons in CA1 could follow up to 50 Hz (Fig. 2g,h). In addition, CA3 interneurons were able to fire continuously in response to prolonged constant blue light (Fig. 2i), and this firing produced synaptic hyperpolarizing current recorded from CA3 pyramidal neurons (Fig. 2j). Collectively, these results demonstrate broad functional ChR2 expression in local inhibitory interneurons distributed throughout the cortex and hippocampus. We also observed light-evoked GABA release from axon terminal fields located within the medial habenula that originate from putative long-range GABAergic projection neurons of the medial septum and nucleus of the diagonal band (Supplementary Fig. 4 and Supplementary Fig. 5)[28].

ChAT-ChR2(H134R)-EYFP transgenic mice

Choline acetyltransferase (ChAT) is the enzyme responsible for acetylcholine synthesis. We targeted ChR2-EYFP to the initiating ATG codon in exon III of the ChAT gene. Three of eighteen founder lines exhibited ChR2-EYFP expression in the brain (Supplementary Table 1). *ChAT-ChR2-EYFP* line 6 showed strong ChR2-EYFP expression in the striatum, basal forebrain, facial nucleus, trochlear nucleus, medial habenula, interpeduncular nucleus (IPN) and various other brainstem motor nuclei (Supplementary Fig. 6 and Supplementary Fig. 7). Low ChR2-EYFP was also observed in the cortex and hippocampus. Co-immunostaining using anti-ChAT and anti-GFP antibodies revealed strong co-localization in cortex (100%), striatum (100%), globus pallidus (100%), and medial habenula (98.2%) (Supplementary Fig. 6b–d and Supplementary Table 3), thus confirming the cholinergic identity of ChR2-EYFP expressing neurons.

We targetd striatal cholinergic neurons for electrophysiological recordings in acute brain slices from adult *ChAT-ChR2-EYFP* line 6 transgenic mice based on their characteristic large somata and membrane targeted ChR2-EYFP fluorescence (Fig. 3a). The majority of recorded neurons exhibited a characteristic tonic firing and pronounced hyperpolarization activated currents (I_h)[29]. Blue light elicited robust photocurrents that in some neurons exceeded 1 nA, indicating very strong ChR2 expression (Fig. 3b). Consequently, these neurons could be driven to fire action potentials in response to patterned light up to 20 Hz (Fig. 3c). Firing became less reliable at frequencies above 20 Hz (data not shown). Due to the powerful abrupt depolarization with light, many neurons exhibited extra spikes following the first elicited action potential in the train (Fig. 3c). Importantly, cell-attached recordings demonstrated that precisely timed action potentials could readily be induced on top of spontaneous tonic firing (Fig. 3d).

We further investigated the functional activation of striatal cholinergic neurons in *ChAT-ChR2-EYFP* line 6 mice *in vivo* by implanting tetrodes together with an optic fiber for

simultaneous electrophysiological recording of neural activity and delivery of precisely patterned blue laser stimulation in awake-behaving mice. Putative striatal cholinergic neuron units were identified by their characteristic tonic spiking activity. A single pulse of blue light delivered over hundreds of identical repeated trials evoked spiking that was time-locked to the stimulus (Fig. 4a). The putative striatal cholinergic neurons exhibited low basal tonic spiking at 3–5 Hz in the absence of photostimulation, and this basal spiking was robustly potentiated by blue light pulses delivered at 30 Hz (Fig. 4b). The measured firing frequency slightly exceeded 30 Hz due to the presence of extra spikes, consistent with the data obtained in acute slice recordings. Importantly, the laser stimulation did not affect our ability to cluster individual neurons based on the differences in waveform shape and size (Supplementary Fig. 8). The capacity to drive spiking with 30 Hz patterned blue light over tens of seconds demonstrates the high reliability of firing that can be achieved *in vivo* and provides evidence that the dynamic range for modulating neuronal firing rates may be broader *in vivo* as compared to *in vitro*.

We examined the influence of striatal cholinergic neuron activity on putative MSN units within striatal circuits *in vivo*. On trials in which the cholinergic neurons were stimulated with 30 Hz blue laser light, putative MSNs showed decreased firing frequency (Fig. 4d; light off trials: 0.65 Hz, light on trials: 0.33 Hz). This finding closely matches the results obtained in a recent study that employed virus-mediated delivery of ChR2 to modulate striatal cholinergic neuron activity *in vivo*[16]. Our findings demonstrate the utility of *ChAT-ChR2-EYFP* line 6 for analysis of complex circuitry in awake-behaving mice.

In *ChAT-ChR2-EYFP* line 6 brain slices we frequently observed that striatal cholinergic neurons entered a state of “depolarization block” of action potential firing with prolonged light presentation, presumably due to strong depolarization induced by ChR2 activation. In light of this observation we also characterized a lower expressing line, *ChAT-ChR2-EYFP* line 5, which has no visible EYFP fluorescence in striatal cholinergic neurons in live slices despite strong signal with antibody enhancement. Nevertheless, clear photocurrents were reliably elicited by blue light (Supplementary Fig. 9a). These responses were an order of magnitude lower than the average responses measured for the same neuronal population in line 6; however, this low ChR2 expression was sufficient to drive significant potentiation of action potential firing in response to sustained blue light (Supplementary Fig. 9b,c). The potentiation of firing rate could be sustained for 30 s or longer in many recorded neurons (Supplementary Fig. 9d). These data demonstrate that *ChAT-ChR2-EYFP* line 5 may be useful for potentiation of basal firing with blue light over tens of seconds, whereas *ChAT-ChR2-EYFP* line 6 will be more useful when precisely timed firing in response to blue light pulses is desirable. In addition, we find that *ChAT-ChR2-EYFP* line 6 (but not line 5) should have even further utility for axon stimulation experiments using blue light—as we have demonstrated for the medial habenula to IPN projection pathway (Supplementary Fig. 10 and Supplementary Fig. 11).

TPH2-ChR2(H134R)-EYFP transgenic mice

The enzyme tryptophan hydroxylase 2 (TPH2) is the rate-limiting enzyme in the synthesis of serotonin (or 5-hydroxytryptamine; 5-HT) in the central nervous system. We engineered

ChR2-EYFP into the ATG site of the first exon of the TPH2 gene. Only one of six founder lines had adequate ChR2-EYFP expression in the brainstem (Supplementary Table 1). Moderate ChR2-EYFP expression was seen in the dorsal raphe nucleus (DRN), median raphe nucleus (MnR), and IPN (Supplementary Fig. 12). TPH2 immunofluorescence strongly co-localized with anti-GFP antibody labeled neurons, (81% for DRN, 87.1% for MnR, and 85% for IPN), confirming the serotonergic identity of ChR2-EYFP+ neurons in this line (Supplementary Fig. 12 and Supplementary Table 3). The ChR2-EYFP+ neurons were virtually all TPH2+ (100% for DRN and MnR, 98.5% for IPN), which suggests that ChR2-EYFP is selectively expressed in serotonergic neurons with no ectopic expression.

We performed electrophysiological recordings of ChR2-EYFP expressing neurons in the DRN in acute brain slices from juvenile mice. 5-HT neurons were identified by their large polymorphic somata, location in the DRN, and expression of EYFP fluorescence at the soma. In many neurons it was possible to visualize brightly fluorescent segments of 5-HT neuronal processes (Fig. 5a). Recorded neurons routinely exhibited basal tonic firing (mean = 2.63 Hz) in our acute slice preparation, similar to rates recorded *in vivo*[30, 31].

Recorded DRN 5-HT neurons responded to blue light with moderate amplitude photocurrents (mean = 158.8 pA, Fig. 5b). Reliable action potential firing could be evoked from DRN 5-HT neurons at up to 20 Hz with patterned blue light, although missed spikes were observed late in the train for some neurons (Fig. 5d,e). We observed variability in the ChR2-EYFP expression levels across the many sampled DRN 5-HT neurons. In particular, some putative 5-HT neurons did not exhibit visible EYFP fluorescence in the live slices. These neurons responded with very weak photocurrents, thus confirming their identity as 5-HT neurons yet with low functional ChR2-EYFP expression (Supplementary Fig. 13). Thus, we focused on further characterizing the sub-population of 5-HT neurons with clearly visible EYFP fluorescence. Importantly, we found that basal tonic firing could be potentiated by short bouts of blue light in a consistent and repeatable manner, and by sustained presentation of blue light up to tens of seconds (Fig. 5f,g,h). We also found that patterned photo-stimulation could override basal tonic firing (Supplementary Fig. 13).

Pvalb-ChR2(H134R)-EYFP transgenic mice

To achieve selective expression of ChR2 in Pvalb+ interneurons, we targeted ChR2-EYFP to the ATG codon in exon II of the Pvalb gene. Six of ten founder lines exhibited detectable ChR2-EYFP expression with nearly identical patterns in the brain (Supplementary Table 1). Pvalb-ChR2-EYFP line 15 was selected for further analysis and showed strong expression throughout the molecular layer of the cerebellum, the TRN and brainstem, and low expression in the thalamus and inferior colliculus (Supplementary Fig. 14a). Co-immunostaining with anti-Pvalb and anti-GFP antibodies further confirmed that these ChR2-EYFP expressing neurons are Pvalb+ interneurons (Supplementary Fig. 14b,c). Notably, despite the known expression of Pvalb in cortical, striatal, and hippocampal interneuron subsets there was no detectable EYFP fluorescence in these areas, likely reflecting the relatively weak activity of the Pvalb promoter in these regions.

We performed electrophysiological recordings in acute brain slices from adult *Pvalb-ChR2-EYFP* mice. We performed extracellular field recordings of putative TRN units located

within the area bounded by clear EYFP fluorescence (Fig. 6a and Supplementary Fig. 14a). TRN units responded to constant blue light presentation with a complex pattern of firing consisting of an initial burst of spikes followed by simple spiking that is the predominant characteristic firing pattern of this neuron type (Fig. 6b,c,d)[32, 33]. Initial burst firing was also elicited by patterned light stimulation; however, the simple spiking portion of the response exhibited perfect fidelity up to the maximum tested frequency of 20 Hz (Fig. 6c).

The *Pvalb-ChR2-EYFP* mice also exhibit very strong EYFP fluorescence in the molecular layer of the cerebellum, suggesting this line may be useful to control neuronal firing in cerebellar circuitry. Thus, Purkinje cells were targeted for recordings based on their characteristic large somata, prominent apical dendrite, and laminar organization in the Purkinje cell layer. These neurons did not exhibit clearly visible somatic EYFP fluorescence in live slices, however, EYFP fluorescence was readily visualized throughout the full extent of the Purkinje cell dendritic tree (Fig. 6e). These neurons exhibited large inward photocurrents in response to blue light (mean = 900.0 pA; Fig. 6f). Purkinje cells were capable of reliable action potential firing in response to patterned blue laser stimulation up to 20 Hz (Fig. 6i,j,k). Missed spikes were rarely observed over the frequencies tested, however, extra spikes were often observed following the initial action potential in a train (Fig. 6j,k). The extra spikes are most likely due to the rapid and pronounced depolarization with light resulting from high ChR2 expression levels or prolonged depolarization following each spike. The powerful depolarization upon ChR2 activation at high laser power was sufficient to induce complex spikes in a subset of Purkinje cells (Fig. 6g). It was determined that the complex spikes consisted of initial simple spikes with superimposed tetrodotoxin-insensitive putative dendritic Ca^{2+} spikes (Supplementary Fig. 15a), and these observations are consistent with known active properties of Purkinje cell dendrites[34].

DISCUSSION

We employed a BAC transgenic strategy to express ChR2-EYFP under the endogenous promoter elements that define the GABAergic, cholinergic, serotonergic, and Pvalb+ subtype of neurons throughout the CNS. While viral vectors have successfully been used by several laboratories to target ChR2 to defined neuronal populations within the intact mouse brain[3–18], there are still important limitations and challenges to these strategies. Every experimental animal requires surgical stereotaxic delivery of virus encoding the ChR2 transgene. Inevitably, not every injected animal is suitable for experimentation due to experimenter error. Even those animals that are deemed suitable may have variable spread of the virus at the injection site, gradients of transgene expression levels in infected brain regions, or potential tissue damage. These potential confounding factors are eliminated by the development and use of cell-type specific ChR2-EYFP transgenic mouse lines. Our mouse lines have robust and functional transgene expression in defined populations of neurons that is stable in terms of both pattern and level of ChR2-EYFP expression across generations.

A recent study described a Cre-inducible ChR2-EGFP knock-in mouse and utilized this line to analyze the organization of cortical interneuron connectivity within neocortical circuits[35]. To achieve functional ChR2-EGFP expression it was necessary to use mice that were

homozygous for the inducible ChR2 allele and heterozygous for *GAD2-CreER*^{T2}, thus demonstrating that this line confers only weak Cre-inducible ChR2 expression. These findings closely match data obtained with a virtually identical mouse line previously developed in our laboratory using the ChR2(H134R) variant (unpub. data). Additional modifications to the strategy, such as those recently implemented for creating improved Cre reporter mice[36], will be required to achieve robust ChR2 expression from a broadly applicable Cre-inducible knock-in allele. Furthermore, we have empirically found that the optimal level of ChR2 expression necessary to achieve dynamic functional manipulation of neuron firing can vary extensively across diverse neuron types, and thus, it may not be possible to achieve optimal ChR2 expression in all neuron types with a single generic inducible ChR2 knock-in allele.

The BAC transgenic strategy achieves the same cell-type specificity as inducible ChR2 alleles combined with Cre driver lines but does not require complicated breeding schemes. These novel transgenic mice will be particularly desirable for investigators utilizing ChR2 to elucidate and potentially correct circuitry dysfunction in existing genetic mouse models of neurological disorders. In such existing models, a significant increase in the complexity of the breeding schemes or delivery techniques for introduction of ChR2 may be prohibitive. Thus, the tools we have developed greatly simplify the experimental paradigms needed to perform optogenetics-based investigations of circuitry function for several important classes of CNS neurons and will make these approaches widely accessible to scientists exploring a diverse range of topics in neurobiology.

METHODS

Methods and any associated references are available in the online version of the Article.

FULL METHODS (ONLINE VERSION)

Antibodies

Rabbit anti-GFP antibody (A11122, 1:1000 dilution) was from Invitrogen, mouse anti-GFP antibody (Mab3580, 1:1000 dilution), mouse anti-GAD67 antibody (Mab5406, 1:1000 dilution), and goat anti-ChAT antibody (AB144P, 1:200 dilution) were from Millipore. Mouse anti-TPH2 antibody (T0678, 1:500 dilution) was from Sigma. Rabbit anti-parvalbumin antibody (PV-28, 1:5000 dilution) was from Swant.

Generation of cell-type specific ChR2-EYFP BAC transgenic mice

The BAC transgenic mice were generated as previously described[37]. Briefly, BAC clones were obtained from Children's Hospital Oakland Research Institute. ChR2-EYFP which contains the H134R mutation was engineered into the ATG exon of the specific BAC clones through homologous recombination (see Supplementary Fig. 1 and Supplementary Table 1 for detailed information). Transgenic mice were generated by the injection of modified BAC DNA constructs into fertilized oocytes, using standard pronuclear injection techniques[38]. Fertilized eggs were collected from matings between C57BL/6J and CBA F1 hybrids. Genotypes were determined by PCR from mouse tail DNA samples (see Supplementary Table 2 for details). PCR-positive animals were kept as founders to establish transgenic lines

by mating to C57BL/6J mice. All research involving mice has been conducted according to the Institutional Animal Care and Use Committee guidelines at Duke University. All procedures were approved by the Institutional Animal Care and Use Committee at Duke University.

Section preparation and imaging

Mouse brain section and imaging were done as previously described[37]. Briefly, mice were anesthetized by the inhalation of isoflurane and were intracardially perfused with Lactated Ringers solution, followed by the fixation of 4% paraformadehyde (PFA). Mouse brains were then post-fixed in 4% PFA overnight at 4 °C. 50 μm sagittal or coronal sections were cut using a vibratome, then mounted and imaged with a ZEISS AxioImager A1 microscope using a 5 × objective or with Nikon PCM2000 confocal microscope using a 20 × objective. Rabbit or mouse anti-GFP antibody was used in co-immunostaining with anti-GAD67, anti-ChAT, anti-TPH2 or anti-parvalbumin antibody. Briefly, sections were blocked with blocking buffer (5% normal goat serum, 2% BSA, 0.2% triton X-100 in PBS) (0.1 M Tris, pH 7.6 was used for anti-GAD67 and anti-ChAT antibodies) for 1 hour at room temperature, then incubated with primary antibody overnight at 4 °C. Following incubation with the primary antibody, sections were washed with either PBS or 0.1 M Tris three times every 20 minutes, followed by incubation with Alex 488 or Cy3 conjugated secondary antibodies for 2–4 hours at room temperature, and then washed with PBS or 0.1 M Tris. Sections were transferred onto slides, dried, mounted with 0.1% paraphenylinediamine in 90% glycerol-PBS (PPD), and imaged with a Nikon PCM2000 confocal microscope.

Equipment and settings

The montage images of the mouse brain sagittal or coronal sections in Supplementary Fig. 2a, 3, 6a, 7, 12a,14a were taken with the ZEISS AxioImager A1 microscope equipped for fluorescence with a FITC filter and an AxioCamHR camera. The software used was AxioVision Rel 4.7 with the following main settings: 5×–1× tube, X-scaling: 1.275 micrometers per pixel, Y-scaling: 1.275 micrometers per pixel, frame-pixel-distance 6.45. The exposure time was 100–200 ms. The montage images were adjusted for brightness and contrast in Photoshop and converted from RGB to CMYK mode.

The confocal images in Supplementary Fig. 2b–d, 6b–d, 12b–d and 14b,c were taken on a Nikon PCM2000 confocal microscope. The objective lens used was 20 ×,0.75 DIC M. The main settings were: large pinhole; first dichroic slider, RGB-red, 505-green; second dichroic slider, 565 for both red and green fluorescence images; ND filter selector, 10% transmission. The software used was Simple PCI 4.06 with the following settings: capture mode, 2× integration; fast scan mode, 1× fast scan; color, PCM2000 1024 color; PMT black level: 350; PMT gain, 1,000–1,500. The confocal TIFF files were equally adjusted for brightness and contrast in Photoshop and cropped to 500 × 500 pixels. Red color was converted to magenta and the image was converted to CMYK mode.

Acute brain slice preparation and electrophysiology

Acute brain slices were prepared from predominantly mature adult (2–8 months) but in some limited cases (e.g. brainstem slices from *TPH2-ChR2-EYFP* mice) from juvenile (21–30 day

old) mice according to our recently reported modified adult brain slice methodology[39] but with a few additional improvements. The mice were deeply anesthetized by intra-peritoneal injection of Avertin (tribromoethanol) and then trans-cardially perfused with 25–30 mL of carbogenated protective artificial cerebrospinal fluid (aCSF) of the following composition: 92 mM N-methyl-D-glucamine (NMDG), 2.5 mM KCl, 1.25 mM NaH_2PO_4, 30 mM $NaHCO_3$, 20 mM HEPES, 25 mM glucose, 2 mM thiourea, 5 mM Na-ascorbate, 3 mM Na-pyruvate, 0.5 mM $CaCl_2.4H_2O$, and 10 mM $MgSO_4.7H_2O$. The pH of the solution was titrated to 7.3–7.4 with concentrated HCl (which provides Cl^- counter-ions for NMDG). HEPES and thiourea plus ascorbate were included as critical components to reduce edema and oxidative damage during slicing, recovery, and extended slice incubation[40, 41]. Mice were then decapitated and the brains were removed into the cutting solution for an additional one minute. The brains were then rapidly embedded in 2% low melt agarose and mounted for either coronal (cortex, hippocampus, olfactory bulb, brain stem, MHb) or sagittal (cerebellum) sectioning at 300 μM thickness on a VF200 model Compresstome (Precisionary Instruments) using a zirconium ceramic injector style blade (Specialty Blades). Acute brain slices containing the habenulo-peduncular pathway were prepared using a special slicing angle of 55–60° off the horizontal axis as shown in Supplementary Fig. 10a and as described recently 42. For midbrain slices containing the DRN the slice thickness was reduced to 200 μM to improve visualization using IR-DIC optics.

Slices were initially recovered for ≤ 20–30 minutes at room temperature (23–25 °C) in carbogenated protective cutting aCSF. In later experiments we refined the procedure by performing this initial recovery at 32–34 °C for ≤ 10–15 min rather than at room temperature, which we found provided improved visualization. The exact duration of the recovery period is critical for obtaining the optimal balance between morphological and functional preservation of the brain slices, and the timing of this recovery step exhibits clear temperature dependence, as indicated above based on extensive empirical testing. Proper implementation of this brief protective recovery step using our NMDG-based aCSF formula greatly reduces initial neuronal swelling during re-warming and enables routine preparation of healthy acute brain slices for targeted whole-cell recordings from mature adult and aging mice. After this initial recovery period the slices were transferred into a holding chamber containing room temperature carbogenated aCSF of the following composition: 119 mM NaCl, 2.5 mM KCl, 1.25 mM NaH_2PO_4, 26 mM $NaHCO_3$, 12.5 mM glucose, 2 mM $CaCl_2.4H_2O$, 2 mM $MgSO_4.7H_2O$. The aCSF was supplemented with 2 mM thiourea, 5 mM Na-ascorbate, and 3 mM Na-pyruvate to improve slice health and longevity, and slices were stored for 1–5 hours prior to transfer to the recording chamber for use. The osmolarity of all solutions was measured at 300–310 mOsm and the pH was maintained at ~7.3 after equilibration under constant carbogenation. In some experiments using juvenile mice the slices were cut using standard methods (standard aCSF instead of NMDG-based aCSF for cutting and recovery). Although the slice quality was deemed to be inferior based on morphological appearance and ease of identifying cells for targeted recordings, the experimental results obtained using this standard method with juvenile mice were indistinguishable and thus were pooled.

The slices were transferred one at a time to the recording chamber of a BX51WI microscope (Olympus) equipped with infra-red DIC optics (900 nm) and epifluorescence. The slices

were constantly perfused with room temperature (22–25 °C) carbogenated recording aCSF at a rate of 4 mL per min. Whole-cell patch-clamp recordings were obtained from visually identified neurons using boroscilicate glass pipettes (King Precision Glass, Inc, Glass type 8250) pulled on a horizontal pipette puller (P-87, Sutter Instruments) to a resistance of 3–4 MΩ when filled with the internal solution containing 145 mM K-Gluconate, 10 mM HEPES, 1 mM EGTA, 2 mM Mg-ATP, 0.3 mM Na^2-GTP, and 2 mM $MgCl_2$. The pH was adjusted to 7.3 with KOH and the osmolarity was adjusted to 290–300 mOsm with sucrose. This internal composition was selected to more readily distinguish spontaneous and light-evoked inhibitory synaptic events as clear outward currents at a holding potential of −50 mV or −60 mV in voltage clamp mode. The reversal potential for Cl^- was experimentally determined to be −75 mV. The theoretical liquid junction potential was calculated at −11 mV and was not corrected.

Neurons expressing ChR2 were identified by visualization of membrane-targeted EYFP fluorescence around the somata of genetically labeled neuron types. A holding command of −60 mV (except where indicated) was applied to the patched cell, and once the whole-cell mode was established the cell was allowed to stabilize for 2–5 minutes. Blue laser light (473 nm) was delivered through a 200 μm diameter optic fiber (Thor Labs) positioned at the slice surface over the recorded neuron. The other end of the optic fiber was coupled to a commutator and then to the laser (Crystal Laser, 100 mW) and the laser power was controlled by an analog dial. The illuminated area was estimated as a 400 μm by 600 μm oval (0.24 mm^2) and this area was used to calculate the power density following direct measurement of the power output at the optic fiber tip using a power meter (Thor Labs). Pulsing of the laser was computer- controlled using custom “optogenetics” stimulation protocols designed in the pClamp 10.2 software. Light-induced inward currents were evoked with blue laser light delivered at 1–100 Hz frequencies (0.05–5 ms pulse duration), or by continuously applying blue laser light over one second or longer. Similar protocols were applied in the current clamp mode to monitor action potential firing of the recorded neurons in response to blue light stimulation from the resting membrane potential. For tonically active neurons (often seen for striatal cholinergic neurons, cerebellar Purkinje cells, and DRN 5-HT neurons) we assessed the ability to induce action potential firing either on top of basal firing rates or after silencing basal firing with the minimal necessary hyperpolarizing current injection. For experiments using *VGAT-ChR2-EYFP* bran slices to assess ChR2 mediated silencing in local circuits, a layer V cortical neuron was recorded in whole-cell current clamp mode and injected continuously with 100–200 pA of depolarizing current to induce tonic firing. Blue laser light was applied to nearby ChR2-expressing cortical interneurons to assess the extent of silencing or hyperpolarization in the layer V pyramidal neuron. Cell-attached recordings were performed in some experiments to monitor action potential firing without disruption of the cytosol. Cell-attached recordings were performed in voltage clamp mode with a zero holding current. Extracellular field recordings were obtained by placement of a glass recording electrode (1–2 MΩ tip) filled with aCSF into the slice and advanced to the depth that allowed discrimination of putative single units based on the response to blue laser light stimulation (in some cases multiple units were apparent).

A Multiclamp 700B amplifier (Molecular Devices Corporation) and Digidata 1440A were used to acquire electrophysiological signals using Clampex 10.2 software (Molecular Devices). The signals were sampled at 20 kHz and low-pass filtered at 2 kHz. The series-resistance was ≤ 25 MΩ and was not compensated. Access to the recorded cells was continuously monitored, and only recordings with stable series resistance were included for analysis. All data analysis was performed in Clampfit 10.2 (Molecular Devices). Values are expressed as mean ± s.e.m. Data were tested for significance using a non-paired student t-test.

Additional acute brain slice electrophysiological recordings were conducted in the Luo laboratory using previously published procedures with only minor modification[42].

In vivo electrophysiology

Mice were deeply anaesthetized with isoflurane and fitted with light-weight headstages for chronic recording with multiple tetrodes in the mouse striatum[43, 44] (Specialty Machining, Wayland, MA). A small opening in the skull and corresponding incision of the dura mater were made to allow entry of seven tetrodes (each made up of twisted 10 μm Ni-Cr wires) and one fiber optic cable (100 to125 μm, attached to a 1.25 mm ferrule) into the brain parenchyma. Both the tetrodes and the fiber optic cable were held individually in a series of nested polyimide tubes. The tubes, attached to microdrives, were held parallel to screws that were used to advance independently each tetrode and the fiber. After a week of post-surgical recovery, the tetrodes and the fiber optic cable were lowered, day by day, through the full dorsoventral extent of the anterior striatum (anterior-posterior + 1.5 mm, medial-lateral +1.2 mm, dorsal-ventral + 1.9 to 3.3 mm) and recordings and stimulation sites were arranged along these trajectories. The tip of the fiber optic cable was kept 0.5 mm above the tips of the tetrodes.

During neuronal recording sessions, a 16 channel preamplifier (1.7 g) connected to lightweight wires (Neuralynx) was attached to the heastage. Neuronal activity recorded on each tetrode channel was sent through the preamplifier with unity gain to two 8-channel programmable amplifiers (gain: 2,000–10,000; filter: 0.6–6 kHz) and then to a Cheetah data-acquisition system (Neuralynx). The spike waveform of each spike was digitized at 32 kHz and stored with a microsecond-precision time stamp. The fiber optic cable was coupled to a 473 nm laser (100 mW, Shanghai Dream Lasers) by connecting its ferrule to the ferrule at the end of the fiber optic cable attached to the laser. A Zirconia sleeve (Doric Lenses) was used to couple the two ferrules. The laser was controlled by a TTL circuit connecting it to a computer running Delphi software. TTL pulses were concurrently sent to the Cheetah data-acquisition system where they received a time stamp and were stored. Laser power was measured before each session through the fiber optic cable that connected the laser to the head stage fiber. The mouse was placed in a circular container (20 cm diameter) for the recording sessions and was allowed to move freely. Typically, each session consisted of 16 trials (40 s each) during which laser-on and laser-off trials were interleaved and separated by a one minute gap. The tetrodes and the fiber optic cable were moved between sessions to maximize the number of unique neurons recorded.

Unit activity containing the spikes of multiple neurons was sorted off-line into putative single units ("clusters") according to multiple spike parameters (e.g., peak height, valley depth, peak time) on the four channels of each tetrode (DataWave Technologies). The accuracy of spike-sorting and the quality of the single units were then evaluated by (a) t-test for spike variability, (b) spike waveform overlays to confirm uniform waveforms for a given unit and different waveforms across units, and (c) autocorrelograms to detect the presence of an absolute refractory period. Based on these tests, clusters containing noise (artifacts and the activity of other units) were excluded from further analyses. All accepted units were classified as putative medium-spiny projection neurons (MSNs) fast-firing (FF) interneurons, or tonically active interneurons (TANs) based on properties of discharge patterns identified by calculating interspike intervals, autocorrelograms, and firing rates[45]. MSN neurons that fired fewer than 150 spikes in a session were not included in any analysis. Histograms are displayed in bins of variable sizes time-locked to the first laser pulse for laser-on trials and the beginning of recording for laser-off trials. The order of trials was interleaved (on-off-on-off…) and the trials were separated by a 1 min gap. A paired t-test was performed to determine statistical significance of the firing rate change between laser-on and laser-off trials.

Supplementary Material

Refer to Web version on PubMed Central for supplementary material.

ACKNOWLEDGMENTS

We thank P. Miao, K. Harley, L. Strickland, and J. Chemla for technical assistance with mouse husbandry and genotyping, Q. Liu and the NeuroTransgenic Lab at Duke University for pronuclear injections of BAC DNA, and other members of the Feng lab for their support. We also thank C. Keller-McGandy for help with histology in the Graybiel lab, and J. Ren and other members of the Luo lab for providing electrophysiology expertise and input. This work was supported by an American Recovery and Reinvestment Act grant from NIMH (RC1-MH088434) to G.F., a NARSAD Young Investigator Award and NIH Ruth L. Kirschstein National Research Service Award (F32MH084460) to J.T.T., and a NIMH grant to A.M.G. (R01 MH060379).

REFERENCES

1. Gradinaru V, et al. Targeting and readout strategies for fast optical neural control in vitro and in vivo. J Neurosci. 2007; 27:14231–14238. [PubMed: 18160630]
2. Huber D, et al. Sparse optical microstimulation in barrel cortex drives learned behaviour in freely moving mice. Nature. 2008; 451:61–64. [PubMed: 18094685]
3. Johansen JP, et al. Optical activation of lateral amygdala pyramidal cells instructs associative fear learning. Proc Natl Acad Sci U S A. 2010; 107:12692–12697. [PubMed: 20615999]
4. Adamantidis AR, Zhang F, Aravanis AM, Deisseroth K, de Lecea L. Neural substrates of awakening probed with optogenetic control of hypocretin neurons. Nature. 2007; 450:420–424. [PubMed: 17943086]
5. Bi A, et al. Ectopic expression of a microbial-type rhodopsin restores visual responses in mice with photoreceptor degeneration. Neuron. 2006; 50:23–33. [PubMed: 16600853]
6. Alilain WJ, et al. Light-induced rescue of breathing after spinal cord injury. J Neurosci. 2008; 28:11862–11870. [PubMed: 19005051]
7. Aponte Y, Atasoy D, Sternson SM. AGRP neurons are sufficient to orchestrate feeding behavior rapidly and without training. Nat Neurosci. 2010; 14:351–355. [PubMed: 21209617]

8. Atasoy D, Aponte Y, Su HH, Sternson SM. A FLEX switch targets Channelrhodopsin-2 to multiple cell types for imaging and long-range circuit mapping. J Neurosci. 2008; 28:7025–7030. [PubMed: 18614669]
9. Cardin JA, et al. Driving fast-spiking cells induces gamma rhythm and controls sensory responses. Nature. 2009; 459:663–667. [PubMed: 19396156]
10. Gradinaru V, Mogri M, Thompson KR, Henderson JM, Deisseroth K. Optical deconstruction of parkinsonian neural circuitry. Science. 2009; 324:354–359. [PubMed: 19299587]
11. Haubensak W, et al. Genetic dissection of an amygdala microcircuit that gates conditioned fear. Nature. 2010; 468:270–276. [PubMed: 21068836]
12. Kravitz AV, et al. Regulation of parkinsonian motor behaviours by optogenetic control of basal ganglia circuitry. Nature. 2010; 466:622–626. [PubMed: 20613723]
13. Sohal VS, Zhang F, Yizhar O, Deisseroth K. Parvalbumin neurons and gamma rhythms enhance cortical circuit performance. Nature. 2009; 459:698–702. [PubMed: 19396159]
14. Stuber GD, Hnasko TS, Britt JP, Edwards RH, Bonci A. Dopaminergic terminals in the nucleus accumbens but not the dorsal striatum corelease glutamate. J Neurosci. 2010; 30:8229–8233. [PubMed: 20554874]
15. Tsai HC, et al. Phasic firing in dopaminergic neurons is sufficient for behavioral conditioning. Science. 2009; 324:1080–1084. [PubMed: 19389999]
16. Witten IB, et al. Cholinergic interneurons control local circuit activity and cocaine conditioning. Science. 2010; 330:1677–1681. [PubMed: 21164015]
17. Cruikshank SJ, Urabe H, Nurmikko AV, Connors BW. Pathway-specific feedforward circuits between thalamus and neocortex revealed by selective optical stimulation of axons. Neuron. 2010; 65:230–245. [PubMed: 20152129]
18. Varga V, et al. Fast synaptic subcortical control of hippocampal circuits. Science. 2009; 326:449–453. [PubMed: 19833972]
19. Arenkiel BR, et al. In vivo light-induced activation of neural circuitry in transgenic mice expressing channelrhodopsin-2. Neuron. 2007; 54:205–218. [PubMed: 17442243]
20. Wang H, et al. High-speed mapping of synaptic connectivity using photostimulation in Channelrhodopsin-2 transgenic mice. Proc Natl Acad Sci U S A. 2007; 104:8143–8148. [PubMed: 17483470]
21. Tomita H, et al. Visual properties of transgenic rats harboring the channelrhodopsin-2 gene regulated by the thy-1.2 promoter. PLoS One. 2009; 4:e7679. [PubMed: 19893752]
22. Hagglund M, Borgius L, Dougherty KJ, Kiehn O. Activation of groups of excitatory neurons in the mammalian spinal cord or hindbrain evokes locomotion. Nat Neurosci. 2010; 13:246–252. [PubMed: 20081850]
23. Dhawale AK, Hagiwara A, Bhalla US, Murthy VN, Albeanu DF. Non-redundant odor coding by sister mitral cells revealed by light addressable glomeruli in the mouse. Nat Neurosci. 2010; 13:1404–1412. [PubMed: 20953197]
24. Chuhma N, Tanaka KF, Hen R, Rayport S. Functional connectome of the striatal medium spiny neuron. J Neurosci. 2011; 31:1183–1192. [PubMed: 21273403]
25. Sagne C, et al. Cloning of a functional vesicular GABA and glycine transporter by screening of genome databases. FEBS Lett. 1997; 417:177–183. [PubMed: 9395291]
26. Gasnier B. The loading of neurotransmitters into synaptic vesicles. Biochimie. 2000; 82:327–337. [PubMed: 10865121]
27. Gunaydin LA, et al. Ultrafast optogenetic control. Nat Neurosci. 2010; 13:387–392. [PubMed: 20081849]
28. Qin C, Luo M. Neurochemical phenotypes of the afferent and efferent projections of the mouse medial habenula. Neuroscience. 2009; 161:827–837. [PubMed: 19362132]
29. Bennett BD, Callaway JC, Wilson CJ. Intrinsic membrane properties underlying spontaneous tonic firing in neostriatal cholinergic interneurons. J Neurosci. 2000; 20:8493–8503. [PubMed: 11069957]

30. Vandermaelen CP, Aghajanian GK. Electrophysiological and pharmacological characterization of serotonergic dorsal raphe neurons recorded extracellularly and intracellularly in rat brain slices. Brain Res. 1983; 289:109–119. [PubMed: 6140982]
31. Liu RJ, Lambe EK, Aghajanian GK. Somatodendritic autoreceptor regulation of serotonergic neurons: dependence on L-tryptophan and tryptophan hydroxylase-activating kinases. Eur J Neurosci. 2005; 21:945–958. [PubMed: 15787701]
32. Lee SH, Govindaiah G, Cox CL. Heterogeneity of firing properties among rat thalamic reticular nucleus neurons. J Physiol. 2007; 582:195–208. [PubMed: 17463035]
33. Huguenard JR, Prince DA. A novel T-type current underlies prolonged Ca(2+)-dependent burst firing in GABAergic neurons of rat thalamic reticular nucleus. J Neurosci. 1992; 12:3804–3817. [PubMed: 1403085]
34. Llinas R, Sugimori M. Electrophysiological properties of in vitro Purkinje cell dendrites in mammalian cerebellar slices. J Physiol. 1980; 305:197–213. [PubMed: 7441553]
35. Katzel D, Zemelman BV, Buetfering C, Wolfel M, Miesenbock G. The columnar and laminar organization of inhibitory connections to neocortical excitatory cells. Nat Neurosci. 2011; 14:100–107. [PubMed: 21076426]
36. Madisen L, et al. A robust and high-throughput Cre reporting and characterization system for the whole mouse brain. Nat Neurosci. 2010; 13:133–140. [PubMed: 20023653]
37. Zhao S, et al. Fluorescent labeling of newborn dentate granule cells in GAD67-GFP transgenic mice: a genetic tool for the study of adult neurogenesis. PLoS One. 2010; 5
38. Feng G, et al. Imaging neuronal subsets in transgenic mice expressing multiple spectral variants of GFP. Neuron. 2000; 28:41–51. [PubMed: 11086982]
39. Peca J, et al. Shank3 mutant mice display autistic-like behaviours and striatal dysfunction. Nature. 2011; 472
40. Brahma B, Forman RE, Stewart EE, Nicholson C, Rice ME. Ascorbate inhibits edema in brain slices. J Neurochem. 2000; 74:1263–1270. [PubMed: 10693960]
41. MacGregor DG, Chesler M, Rice ME. HEPES prevents edema in rat brain slices. Neurosci Lett. 2001; 303:141–144. [PubMed: 11323105]
42. Ren J, et al. Habenula “Cholinergic” Neurons Corelease Glutamate and Acetylcholine and Activate Postsynaptic Neurons via Distinct Transmission Modes. Neuron. 2011; 69:445–452. [PubMed: 21315256]
43. Jog MS, et al. Tetrode technology: advances in implantable hardware, neuroimaging, and data analysis techniques. J Neurosci Methods. 2002; 117:141–152. [PubMed: 12100979]
44. Kubota Y, et al. Stable encoding of task structure coexists with flexible coding of task events in sensorimotor striatum. J Neurophysiol. 2009; 102:2142–2160. [PubMed: 19625536]
45. Barnes TD, Kubota Y, Hu D, Jin DZ, Graybiel AM. Activity of striatal neurons reflects dynamic encoding and recoding of procedural memories. Nature. 2005; 437:1158–1161. [PubMed: 16237445]

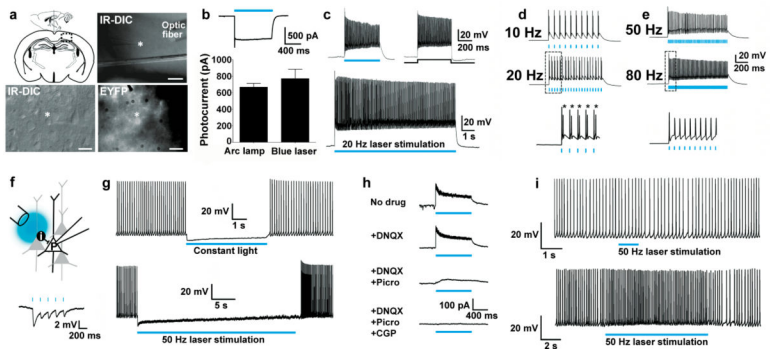

Figure 1.

Functional characterization of *VGAT-ChR2(H134R)-EYFP* BAC transgenic mice. (**a**) Diagram of acute coronal brain slice preparation containing the cortex and representative image showing placement of the optic fiber in the region of recorded cortical interneurons (asterisk) (top). Scale bar: 200 μm. High magnification IR-DIC and EYFP fluorescence image of a layer V interneuron (bottom). Scale bar: 20 μm. (**b**) Voltage clamp recording demonstrating photocurrents induced by blue laser light (26.3 mW mm^{-2}) (top). Plot of peak steady-state photocurrent in response to blue light delivered as indicated (bottom). (**c**) Current clamp mode recording showing firing of a single neuron in response to blue light or to +400 pA current injection (top), or to prolonged 20 Hz stimulation (0.52 mW mm^{-2}, 1 ms pulse width) (bottom). (**d**) Current clamp mode recording demonstrating action potential firing in response to patterned blue laser light stimulation (2.1 mW mm^{-2}, 1 ms pulse width) (top and middle). An expanded view of initial action potential firing at 20 Hz demonstrating extra spikes (asterisks) is shown (bottom). (**e**) Reliable action potential firing of the same interneuron to patterned blue laser light stimulation at 50 Hz (top) and 80 Hz (middle). Expanded view of firing at 80 Hz is shown (bottom). (**f**) Diagram of recording configuration to test functional effect of light-induced interneuron firing in cortical microcircuits (top). Current clamp mode recording of a layer V pyramidal neuron showing hyperpolarization in response to 5 Hz blue laser stimulation (2.1 mW mm^{-2}, 1 ms) (bottom). (**g**) Robust silencing of layer V pyramidal neuron firing in response to constant blue light (top) or 50 Hz blue laser stimulation (473 nm, 2.1 mW mm^{-2}, 1 ms pulse width) (bottom). Action potential firing was induced by constant +150 pA direct current injection. (**h**) Voltage clamp recording of the same layer V pyramidal neuron in the absence (no drug) and presence of the indicated compounds. The blue bar indicates 50 Hz blue laser stimulation. (**i**) Response of the same neuron to 50 Hz blue laser light (2.1 mW mm^{-2}, 1 ms pulse width) for 1 s (top) or 10 s (bottom) during co-application of GABA-A and GABA-B receptor antagonists.

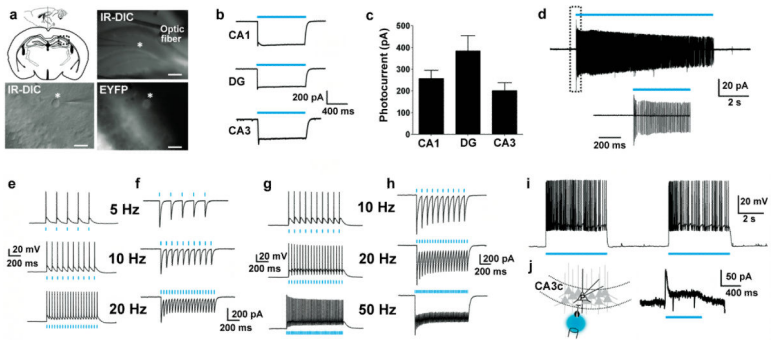

Figure 2.

Functional characterization of hippocampal interneurons in *VGAT-ChR2(H134R)-EYFP* BAC transgenic mice. (**a**) Diagram of acute coronal brain slice preparation containing the hippocampus and representative image showing placement of the optic fiber in the region of a recorded hippocampal interneuron (asterisk) (top). Scale bar: 200 μm. High magnification IRDIC and fluorescence image of an interneuron in the dentate gyrus molecular layer (bottom). Scale bar: 20 μm. (**b**) Example photocurrents induced by blue laser light (26.3 mW mm^{-2}) in various hippocampal regions. (**c**) Plot of peak steady-state photocurrent in response to blue light for interneurons in various hippocampal regions. (**d**) Cell-attached recording of a dentate gyrus interneuron demonstrating firing in response to 10 s blue light stimulation (top). An expanded view is shown (bottom). (**e, f**) Current clamp mode (e) and voltage clamp (f) recording of a dentate gyrus interneuron in response to patterned blue laser stimulation as indicated (2.1 mW mm^{-2}, 1 ms pulse width). (**g, h**) Current clamp mode (g) and voltage clamp (h) recording of a CA1 interneuron showing the response to patterned blue laser stimulation at 10, 20 and 50 Hz (2.1 mW mm^{-2}, 1 ms pulse width). (**i**) Current clamp mode recording of a CA3 interneuron showing sustained action potential firing in response to repeated bouts of constant blue light. (**j**) Diagram of recording configuration to test functional effect of light-induced interneuron firing in the CA3c subfield circuitry (left) and voltage clamp recording of a CA3c pyramidal neuron demonstrating outward current in response to blue light (right).

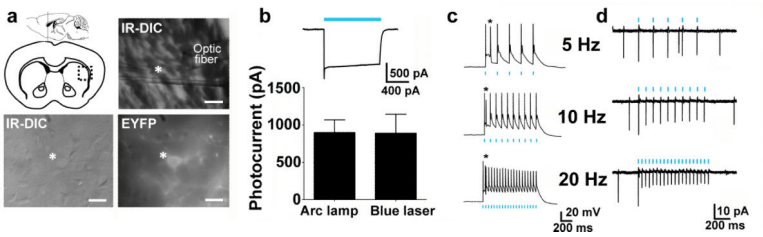

Figure 3.

Functional characterization of *ChAT-ChR2(H134R)-EYFP* line 6 BAC transgenic mice. (**a**) Diagram of acute coronal brain slice containing the dorsal striatum and a representative image showing placement of the optic fiber in the region of a recorded neuron (top). Scale bar: 200 μm. IR-DIC and EYFP fluorescence image of a recorded striatal cholinergic neuron (bottom). Scale bar: 20 μm. (**b**) Voltage clamp recording demonstrating inward current induced by blue laser light (26.3 mW mm^{-2}) (top). Summary plot of peak steady-state photocurrent in response to blue light delivered as indicated (bottom). (**c**) Action potential firing in response to patterned blue laser light (5.21 mW mm^{-2}, 5 ms pulse width). Asterisks indicate extra spikes. A small hyperpolarizing current injection was applied to silence basal firing. (**d**) Cell-attached recording of firing in response to patterned blue laser light (2.1 mW mm^{-2}, 5 ms pulse width). Light stimuli were delivered on top of basal tonic firing.

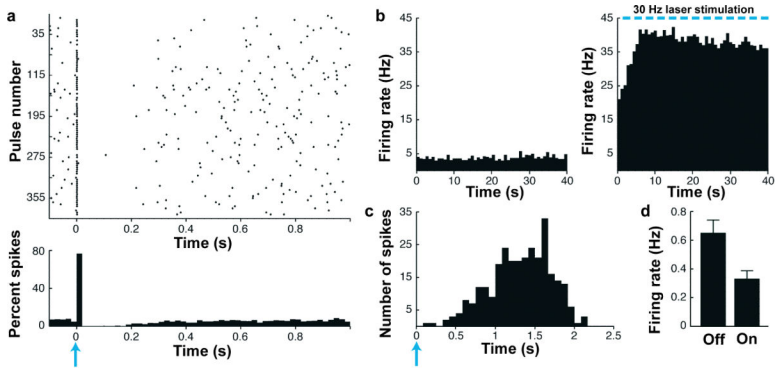

Figure 4.

In vivo straital electrophysiology for *ChAT-ChR2-EYFP* line 6 BAC transgenic mice. (**a**) Raster (top) and spike-density histograms (bottom) of a striatal cholinergic neuron in response to a single pulse of blue laser light (10 mW, 18 ms pulse width, blue arrow) over repeated trials. (**b**) Spike-density histogram of a striatal cholinergic neuron in response to 40 s blue laser light stimulation (10 mW, 18 ms pulse width) at 30 Hz frequency. (**c**) Spike-density histogram of a striatal cholinergic neuron showing rapid response (1–2 ms) to blue laser light stimulation (10 mW, 18 ms pulse width, blue arrow). (**d**) Bar graph of putative medium spiny neuron firing rate in response to 40 s blue laser light stimulation (10 mW, 18 ms pulse width) at 30 Hz ($n = 20$, $P < 0.01$).

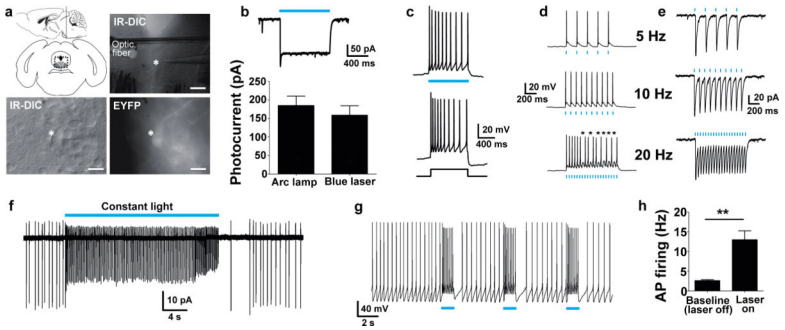

Figure 5.

Functional characterization of *TPH2-ChR2(H134R)-EYFP* BAC transgenic mice. (**a**) Diagram of acute coronal brainstem slice preparation and representative image showing placement of the optic fiber in the region of a recorded neuron (top). Scale bar: 200 μm. IR-DIC and EYFP fluorescence image of a recorded 5-HT neuron in the dorsal raphe nucleus (bottom). Scale bar: 20 μm. (**b**) Voltage clamp recording of a 5-HT neuron demonstrating inward current induced by blue laser light (26.3 mW mm^{-2}) (top). Plot of peak steady-state photocurrent in response to blue light delivered as indicated (bottom). (**c**) Current clamp mode recording showing action potential firing in response to blue laser light (26.3 mW mm^{-2}) (top) or in response to +100 pA current injection (bottom). (**d–e**) Current clamp mode (d) and voltage clamp (e) recording of responses to patterned blue laser light (26.3 mW mm^{-2}, 5 ms pulse width). Asterisks indicate missed action potentials. Note: in panels c–d a small hyperpolarizing current injection was applied to silence basal firing. (**f, g**) Cell-attached recording of a 5-HT neuron under prolonged constant blue light stimulation (f) or to repeated bouts of blue light (g). (**h**) Summary plot of baseline and blue light-induced firing rates. ** $P < 0.01$ (one-tailed paired t-test).

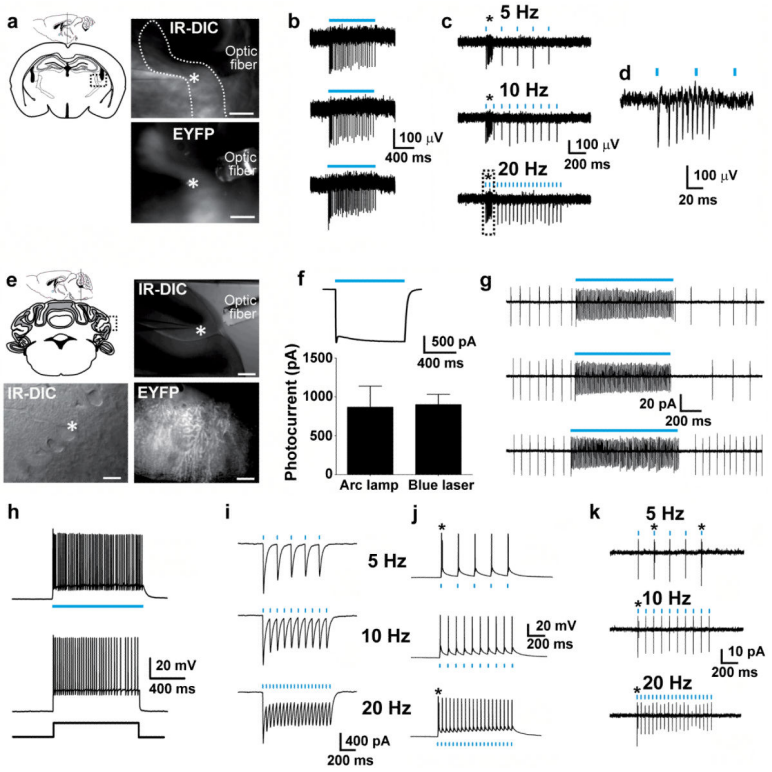

Figure 6.

Functional characterization of *Pvalb-ChR2(H134R)-EYFP* BAC transgenic mice. (**a–e**) Characterization of ChR2-EYFP positive neurons in the thalamic reticular nucleus (TRN). (**a**) Diagram of a coronal brain slice containing the TRN and representative image showing placement of the optic fiber (top) and EYFP fluorescence (bottom) in the region of recorded neurons. Scale bar: 200 µm. (**b**) Extracellular field recordings of a putative single TRN neuron that was silent at rest in response to blue laser light at 10.5 mW mm^{-2} (top) and 26.3 mW mm^{-2} (middle), or delivered from a mercury arc lamp (bottom). (**c**) Extracellular field recording of action potential firing in response to patterned blue laser light (26.3 mW mm^{-2}, 5 ms pulse width). Asterisks indicate initial burst firing. (**d**) Expanded view of lower panel in c. (**e–k**) Characterization of ChR2-EYFP expressing cerebellar Purkinje cells. (**e**) Diagram of an acute brain slice containing the cerebellum and representative slice image showing placement of the optic fiber in the region of a recorded neuron in the Purkinje cell layer (top). Scale bar: 200 µm. IR-DIC image and EYFP fluorescence image of a recorded Purkinje cell (bottom). EYFP fluorescence was not easily detected in the Purkinje cell somata due to saturating EYFP fluorescence of the Purkinje cell dendrites in the adjacent molecular layer. Scale bar: 20 µm. (**f**) Voltage clamp recording demonstrating inward current induced by blue laser light (26.3 mW mm^{-2}) (top). Summary plot of peak steady-state photocurrent in response to blue light delivered as indicated. (bottom). (**g**) Cell-attached recordings demonstrating potentiation of baseline firing in response to blue laser light at 1.05 mW mm^{-2} (top), 26.3 mW mm^{-2} (middle), and 157.9 mW mm^{-2} (bottom). (**h**) Current clamp mode recording showing firing in response to blue light (top) or to +400 pA current injection (bottom). (**i,j**) Voltage clamp (i) and current clamp mode (j) recording demonstrating responses to patterned blue laser light (26.3 mW mm^{-2}, 5 ms pulse width).

Asterisks indicate initial doublet firing. Note: a small hyperpolarizing current injection was applied to silence basal firing. (**k**) Cell-attached recording of action potential firing from a single neuron in response to patterned blue laser light (26.3 mW mm^{-2}, 5 ms pulse width). Asterisks indicate doublet firing. This recorded Purkinje cell was silent at rest.